

Accepted for the publication in the *Astrophysical Journal*

Evolutionary Status of SNR 1987A at the Age of Eighteen

Sangwook Park

Department of Astronomy and Astrophysics, 525 Davey Lab., Pennsylvania State University, University Park, PA. 16802

park@astro.psu.edu

Svetozar A. Zhekov¹

JILA, University of Colorado, Box 440, Boulder, CO. 80309

David N. Burrows, Gordon P. Garmire, Judith L. Racusin

Department of Astronomy and Astrophysics, 525 Davey Lab., Pennsylvania State University, University Park, PA. 16802

and

Richard McCray

JILA, University of Colorado, Box 440, Boulder, CO. 80309

ABSTRACT

~18 yr after the supernova explosion, the blast wave of SNR 1987A is entering the main body of the equatorial circumstellar material, which is causing a dramatic brightening of the remnant. We recently reported the observational evidence for this event from our *Chandra* data (Park et al. 2005b; P05 hereafter). We present here the temporal evolution of the X-ray emitting shock parameters and the detailed description of the spectral and image analysis of SNR 1987A, on which P05 was based. While the remnant becomes brighter, the softening of the overall X-ray spectrum continues and is enhanced on around day ~6200 (since the explosion). The two-component shock model indicates that the electron temperatures have been changing for the last ~6 yr. The X-ray spectrum is now

¹Current address: The Space Research Institute, Moskovska str. 6, Sofia-1000, Bulgaria

described by $kT \sim 0.3$ keV and 2.3 keV thermal plasmas which are believed to characteristically represent the shock-heated density gradient along the boundary between the HII region and the dense inner ring. As the blast wave sweeps through the inner circumstellar ring shining in X-rays, we expect that the shock parameters continue to change, revealing the density and abundance structure of the inner ring. Follow-up *Chandra* observations will thus uncover the past history of the progenitor’s stellar evolution. The origin of the relatively faint hard X-ray emission ($E > 3$ keV) from SNR 1987A is still unclear (thermal vs. nonthermal). Considering the continuous brightening of the hard band intensity, as well as the soft band flux, follow-up monitoring observations will also be essential to reveal the origin of the hard X-ray emission of SNR 1987A.

Subject headings: supernovae: general — supernovae: individual (SN 1987A) — supernova remnants — X-rays: general — X-rays: stars

1. INTRODUCTION

We continue to monitor the X-ray remnant of supernova (SN) 1987A with the Advanced CCD Imaging Spectrometer (ACIS) on board *Chandra X-Ray Observatory*. As of 2005 July, we have performed a total of 13 observations, including a pair of deep gratings observations. Results from the first eight ACIS imaging observations have been reported in the literature (Burrows et al. 2000; Park et al. 2002; Park et al. 2004; Park et al. 2005a). We have also presented the results from the high resolution X-ray spectroscopic studies of SNR 1987A using deep *Chandra* gratings observations (Michael et al. 2002; Zhekov et al. 2005; Zhekov et al. 2006).

These studies revealed that the soft X-ray emission of SNR 1987A originates from the shocked hot gas between the forward and reverse shock of the blast wave, which appears as a ring-like morphology with the high resolution ACIS images. The X-ray emitting hot gas is primarily distributed in the “disk” containing the dense equatorial inner ring that was produced by asymmetric stellar winds from the massive progenitor star before the SN (Burrows et al. 1995; Lundqvist & Fransson 1991; Luo & McCray 1991). As the shock sweeps up continuously increasing amount of circumstellar material (CSM), the soft X-ray intensity has thus been rapidly increasing. The overall X-ray spectrum is described by two thermal components, which characteristically represents the decelerated shock front ($kT \sim 0.2$ keV) entering the dense protrusions of the inner ring and the fast shock ($kT \sim 2.5$ keV) propagating into less dense medium.

The recent *Chandra* data indicate that the soft X-ray lightcurve of SNR 1987A has been even more rapidly increasing than ever since early 2004 (day ~ 6200 since the SN). The decelerated, soft component of the shock ($kT \sim 0.3$ keV) begins to dominate the observed 0.5 – 2 keV band X-ray flux at the same epoch. The soft X-ray images also show a global brightening, rather than local intensity increases, during the same period. We interpret that these latest results are indications of the blast wave now interacting all the way around the inner ring rather than with only a few small dense protrusions primarily in the eastern side of the remnant. We have recently reported these new results of the soft X-ray lightcurve and its implications (Park et al. 2005b, P05 hereafter). This is an exciting event that was predicted to occur in $\sim 10 - 20$ yr after the SN (e.g., Luo et al. 1994). The recent high resolution X-ray spectroscopy with the deep *Chandra* gratings observations consistently supports this new evolutionary phase of SNR 1987A (Zhekov et al. 2005; Zhekov et al. 2006). In this paper, we present the data analysis of all up-to-date ACIS observations of SNR 1987A, on which the results of P05 were based, and discuss how the X-ray remnant is evolving as of 2005 July (~ 18 yr after the SN).

2. OBSERVATIONS & DATA REDUCTION

All 13 *Chandra* observations of SNR 1987A are presented in Table 1. The results from the gratings observations are presented in the literature (Michael et al. 2002; Zhekov et al. 2005; Zhekov et al. 2006). We present the results from the 11 undispersed ACIS observations in this work. We reduce these data following the methods described in our previous work (Burrows et al. 2000; Park et al. 2002). We screened all 11 data sets with the flight timeline filter and turned off the pixel randomization for the highest possible angular resolution. We then corrected the spatial and spectral degradation of the ACIS data caused by radiation damage, known as the charge transfer inefficiency (CTI; Townsley et al. 2000), with the methods developed by Townsley et al. (2002a), before further standard data screening by status, grade, and energy selections. “Flaring” pixels were removed and *ASCA* grades (02346) were selected. Photons between 0.3 keV and 8.0 keV were extracted for the data analysis. Lightcurves around the source region were examined for possible contamination from variable background emission. Overall, no severe variability was found. With ObsID 5580, there was moderately flaring background (by a factor of ~ 2) for the entire S3 chip for a short time period of ~ 700 s. Although this flaring background was negligible for the small source region, we excluded this ~ 700 s time interval from the data analysis. The pileup fraction has been small ($< 10\%$) and thus was ignored in the analysis. However, considering the rapid brightening of SNR 1987A, we used subarrays for the latest 3 ACIS observations (Table 1) in order to avoid potential pileup effects.

We then applied the “sub-pixel resolution” method (Tsunemi et al. 2001) to improve the angular resolution of the images to better than the CCD pixel size ($0''.492$). A typical improvement in the angular resolution by $\sim 10\%$ is expected from this method (Mori et al. 2001). The angular size of SNR 1987A is small (the inner ring is only about $1''.6$ across; e.g., Burrows et al. 1995; Jakobsen et al. 1991), and the ACIS detector pixel size is not adequate to fully resolve the remnant. In order to further improve the effective angular resolution of the ACIS images, we deconvolved the images with the detector point spread function using a maximum likelihood algorithm (Richardson 1972; Lucy 1974) as described in our previous work (Burrows et al. 2000).

3. X-RAY MORPHOLOGY

X-ray images of SNR 1987A from our 11 *Chandra*/ACIS observations are presented in Figure 1. The continuous brightening of the X-ray emission from the SNR, particularly from the western side in the recent images in addition to the eastern side, is evident. Our early *Chandra* observations showed that the bright soft X-ray spots in the eastern side of the remnant were positionally coincident with the bright optical spots which were then also dominating in the eastern parts of the inner ring (Burrows et al. 2000; Park et al. 2002). Since then, the optically bright spots have been emerging in the western parts of the inner ring in addition to the eastern portions (Sugerman et al. 2002). The current X-ray images also reveal bright X-ray emission from all around the inner ring. These X-ray and optical data suggest that the blast wave shock is now engulfing areas around the entire inner ring several years after reaching the first local protrusions in the eastern side. In fact, the latest optical and X-ray bright spots show excellent positional correlations (Figure 2). As of 2005 July, the overall surface brightness is an order of magnitude higher than it was in 2000 January. A dramatic brightening of SNR 1987A, caused by the interaction of the blast wave with the dense inner ring, has been predicted to occur around 1999–2007 (Luo & McCray 1991; Luo et al. 1994; Chevalier & Dwarkadas 1995; Borkowski et al. 1997). More recently, based on the radial expansion of the radio remnant of SN 1987A, Manchester et al. (2002) predicted that this event may happen in 2004 ± 2 . Our *Chandra* images indicate that the predicted brightening is now underway (see P05 for more discussion).

The radial expansion of the X-ray remnant of SN 1987A ($v \sim 4000 - 5000 \text{ km s}^{-1}$) has been detected with the earlier *Chandra*/ACIS images (Park et al. 2002; Park et al. 2004). We continue to measure the radial expansion with the new X-ray images. While the X-ray remnant is continuously expanding with an average rate of $v \sim 3200 \text{ km s}^{-1}$, the expansion rate has evidently decelerated down to $v \sim 1600 \text{ km s}^{-1}$ since day ~ 6200 (Racusin et al.

2006, in preparation). This turnover in the expansion rate is indeed expected assuming that the bulk of the X-ray emission originates from the interaction between the blast wave and the inner ring. Because the blast wave is rapidly approaching the dense CSM “wall” of the inner ring’s main body, a significant deceleration of the overall shock velocity is eventually anticipated. The detailed description and the results from our measurements of the radial expansion rate are presented elsewhere (Racusin et al. 2006 in preparation).

The broad-subband images consequently become indistinguishable between the soft ($E = 0.3 - 0.8$ keV) and the hard ($E = 1.2 - 8.0$ keV) bands (Figure 3). This is in contrast to the early subband images which clearly exhibited distinctive differences in bright X-ray spots between the soft and the hard bands (Park et al. 2002).

4. SPECTRAL ANALYSIS

Unlike the early data, which could be described by a $kT \sim 3$ keV thermal plasma (e.g., Park et al. 2002), the recent data of SNR 1987A cannot be adequately fitted by a single shock model. For instance, although the overall spectral shape of the latest data (2005 July) may be described with a $kT \sim 1.5$ keV plasma, the fit is statistically unacceptable ($\chi^2/\nu = 283.4/130$). The poor fit is primarily caused by the infeasibility of the single shock model to properly fit the line features in the soft band ($E < 1.5$ keV). This change is most likely because of the complex shock structure that has recently developed due to the significant interaction between the blast wave and the ambient density gradient (Park et al. 2004; Zhekov et al. 2006). We thus perform spectral analysis of SNR 1987A utilizing two-component plane-parallel shock model (Borkowski et al. 2001), following the methods used in our previous work (Park et al. 2004). Albeit admittedly simplified, we confirm that the two-shock model provides a good approximation for the complex velocity/temperature distribution of the blast wave by characteristically representing the fast and decelerated shocks (Zhekov et al. 2006).

We extract the source spectrum of SNR 1987A from a circular region with a $2''-3''$ radius for each observation. The background spectrum is estimated from a surrounding annulus with an inner radius of $3''.5-4''$ and an outer radius of $7''.5-10''$. Each spectrum has been binned to contain a minimum of 20–50 counts per channel. For the spectral analysis of our CTI-corrected data, we have utilized the response matrices appropriate for the spectral redistribution of the CCD, as generated by Townsley et al. (2002b). We use non-equilibrium ionization (NEI) shock models (`vpshock` in conjunction with the NEI version 2.0 in the `XSPEC`) which are based on `ATOMDB` (Smith et al. 2001). Inner-shell processes are added in this atomic database, which is important for the NEI plasma yet missing in the

current XSPEC NEI version 2¹. We also regenerated the ancillary response functions using the ACIS caldb version 3.00 for all eleven observations in order to consistently correct for the quantum efficiency degradation of the ACIS over the ~ 6 yr period of the observations.

The spectral contributions of the line emission from the elements He, C, Ca, Ar, and Ni are insignificant in the fitted energy range (0.4–5.0 keV), thus we fix the abundances of these elements at previous measurements. He (= 2.57, hereafter, the abundances are relative to solar (Anders & Grevesse 1989)) and C (= 0.09) are set to the abundances of the inner ring (Lundqvist & Fransson 1996). We fix the Ca (= 0.34), Ar (= 0.54) and Ni (= 0.62) abundances to values appropriate for the LMC ISM (Russell & Dopita 1992) because the ring abundances were unavailable for these elemental species in Lundqvist & Fransson (1996). Abundances of other species, N (= 0.76), O (=0.09), Ne (= 0.29), Mg (= 0.24), Si (= 0.28), S (=0.45), and Fe (= 0.16), are fixed at values that we measured with the recent deep *Chandra*/Low Energy Transmission Gratings Spectrometer (LETG) observations (Zhekov et al. 2006), because the high resolution gratings spectrum should provide the most reliable measurements of the abundances. We fix the redshift of SNR 1987A at the value for the LMC ($v = 286 \text{ km s}^{-1}$; Michael et al. [2002]; Zhekov et al. [2005] and references therein).

The eleven individual spectra of SNR 1987A represent a wide range in photon statistics (~ 600 – 27000 counts) with temporal evolution of the shock parameters. In order to make reliable comparisons of the shock parameters among the individual observations, it is essential to determine the foreground absorption, which should be constant over the ~ 6 yr observation period. We found that the N_H measurement is particularly important for reliable measurements of the shock parameters of the early observations with low photon statistics. In order to make the most reliable estimate of the foreground column N_H , we fit all 11 spectra simultaneously, varying the electron temperature, ionization timescale, and the normalization freely among the individual observations. We fit N_H , but tie it to be the same for all individual epochs. The best-fit N_H toward the entire SNR 1987A is $2.35^{+0.09}_{-0.08} \times 10^{21} \text{ cm}^{-2}$ ($\chi^2/\nu = 1058.5/1015$; the uncertainties are with a 90% confidence). We then repeat the spectral fitting for each eleven individual spectrum with N_H and elemental abundances fixed at the values obtained above. We display the ACIS spectrum of SNR 1987A in two representative epochs of 2000 January and 2005 July in Figure 4. The modeled shock parameters from these spectral fits are presented in Table 2. The ionization timescale ($n_e t$) for the soft component is high at all epochs and is not well constrained with lower limits of $n_e t \gtrsim 10^{12} \text{ cm}^{-3} \text{ s}$. The soft component $n_e t$ is thus not explicitly presented in Table 2.

¹The unpublished version of the updated model has been provided by K. Borkowski.

5. Discussion

The X-ray morphology of SNR 1987A has been evolving from a faint, partial ring with a pair of relatively bright spots in the eastern side, to a bright, complete ring over the last ~ 6 yr. Based on the standard picture of the SNR 1987A system, these morphological changes are indeed expected as the blast wave encounters an increasing number of protrusions of the dense inner ring and eventually sweeps through the main body of the entire inner ring. This exciting phase of SNR 1987A’s evolution is highlighted by the recent upturn in the soft X-ray lightcurve. The evolution of the X-ray luminosity of SNR 1987A is presented in Table 3. It is remarkable that the soft X-ray ($E = 0.5 - 2$ keV) flux increase rate has turned up since day ~ 6200 (Figure 5, also see Figure 1 in P05). This soft X-ray lightcurve is interpreted as evidence for the blast wave reaching the entire inner ring at around day ~ 6200 . The detailed description and discussion of the lightcurve analysis can be found in P05. P05 also found observational evidence that independently supports this interpretation, such as the morphological changes in the soft X-ray intensity ratios and the changes in the fractional contribution from the decelerated shock for the observed soft X-ray flux since day $\sim 6000 - 6200$. Racusin et al. (2006, in preparation) reports an apparent deceleration of the radial expansion rate of the SNR since day ~ 6200 , which is self-consistent with our results. The low shock velocities ($v < 1700$ km s $^{-1}$) deduced from the line broadenings obtained with the recent deep *Chandra*/LETG observations of SNR 1987A (Zhekov et al. 2005) were also supportive of the conclusions by P05. The recent mid-IR observations revealed a similar upturn in the IR intensity at around the same epoch of day ~ 6000 (Bouchet et al. 2006). The high resolution mid-IR images show that the bulk of IR emission originates from the inner ring, being consistent with the soft X-ray and optical emission. These IR observations thus also support our interpretation of the blast wave now interacting with the main portion of the dense inner ring.

The X-ray spectrum can be described by two components: e.g., as of 2005 July, the soft ($kT \sim 0.3$ keV) and the hard ($kT \sim 2.3$ keV) components characteristically representing the decelerated and the fast shocks, respectively. The soft component appears to be in (or close to) collisional ionization equilibrium (CIE) with high ionization timescales ($n_e t \gtrsim 10^{12}$ cm $^{-3}$ s), while the hard component is in NEI condition ($n_e t \sim 2 - 3 \times 10^{11}$ cm $^{-3}$ s). These results are consistent with our physical picture of the X-ray emission from the shock interacting with the dense CSM with complex density structure: i.e., on average, for the last several years, the soft component represents the decelerated shock interacting with the dense CSM and the hard component indicates the *undecelerated*, fast shock propagating into the less dense medium. We however note that, recently, the observed 0.5 – 2 keV band emission is dominated almost entirely by emission from the shocked dense CSM (P05). This suggests that even the fast shock component ($kT \sim 2.3$ keV) of the observed 0.5 – 2 keV band X-ray

emission now originates primarily from the “reflected” shock close to the inner ring rather than from the shocked HII region (Zhekov et al. 2005) (also see Figure 3 in Michael et al. 2000). In this picture, the decelerated shock component ($kT \sim 0.3$ keV) of the $0.5 - 2$ keV flux is produced by the “transmitted” shock front into the dense inner ring. The nature of these shock components are discussed in detail with the high spectral resolution LETG data (Zhekov et al. 2005; Zhekov et al. 2006). In the current work, we focus our discussion on the temporal evolution of these shock components.

The overall X-ray spectrum of SNR 1987A has been continuously softening, particularly since day ~ 6200 (Figure 6). The significant change in the softness of the spectrum suggests that a large portion of the shock started to interact with the dense CSM since day ~ 6200 . The electron temperature of the fast shock component has been decreasing whereas that of the soft, decelerated shock component is increasing (Table 2 & Figure 7). This “merging” of two characteristic temperatures may be interpreted as a “transitioning” effect that the increasing fraction of the low-energy tail of the fast shock emission apparently shifts into the hard-tail of the slow shock spectrum. While the separation between the two characteristic electron temperatures becomes smaller, the overall softening of the X-ray spectrum, as reported in the literature (Park et al. 2004; Park et al. 2005a), continues. As of 2005 July, the overall X-ray spectral shape roughly corresponds, on average, to a $kT \sim 1.5$ keV plasma, whereas it was $kT \sim 3$ keV in 2000 January (Burrows et al. 2000; Park et al. 2002). This evolution of the electron temperature is consistent with our interpretation that a large fraction of the shock front has begun interacting with a significant density gradient between the less dense HII region and the dense inner ring. As the blast wave eventually sweeps through the main portions of the dense inner ring, the X-ray spectrum may be dominated by the density structure of the inner ring itself. For instance, if the inner ring has a relatively *uniform* density, one might expect that the observed X-ray spectrum would become properly described by a single, average electron temperature in the future.

The volume emission measures (EM) for both shock components continue to significantly increase (Table 2). This result is in agreement with the increasing contribution from the reflected shock in the fast shock component of the X-ray emission: i.e., the continuously increasing amount of the soft X-ray emission from the fast shock component is originating from the shock entering the strong density gradient near the boundary of the inner ring, rather than from the shocked tenuous HII region. As the blast wave enters a density gradient, the electron temperature of the shocked plasma is inversely correlated with the density ($T \propto n^{-1}$). The evolution of the electron temperature ratio between the fast and decelerated shocks (Figure 7) then implies changes in the density ratio from $n_{slow}/n_{fast} \sim 15$ (day ~ 4700) to ~ 7 (day ~ 6700). While the EMs are increasing for both shock components, their relative ratio has been showing no significant changes with an average ratio of ~ 7.3 (Figure 8). This

means that the X-ray emitting volume ratio has been changing from $V_{fast}/V_{slow} \sim 30$ (day ~ 4700) to ~ 7 (day ~ 6700).

The density ratio between the inner ring and the HII region was estimated to be $\sim 18 - 30$ with the previous *Chandra* data (Park et al. 2004). Considering the simple modeling and various geometrical assumptions embedded in the density estimates, these density ratios were concluded to be consistent with those (~ 100) derived from the UV data (Chevalier & Dwarkadas 1995; Lundqvist & Fransson 1996). With the significantly improved X-ray data (both in quantity and quality) and physically more realistic modeling than Park et al. (2004) utilized, we now consider that the relatively low density ratios derived with the X-ray data may represent some actual physical implications. In other words, our *Chandra* observations presented in this work have been performed since early 2000, ~ 3 yr after the emergence of the optical Spot 1. The emergence of the optical Spot 1 marks the beginning of the significant interaction of the blast wave with the dense CSM along the inner ring. Therefore, even the earliest data of our *Chandra* observations would have been affected by the density gradient in the vicinity of the inner ring, even for the fast shock component. In such a case, it is not surprising to obtain less density contrast between the fast and the decelerated shock components from the X-ray data, compared with the inner ring to HII region density ratios measured by the UV/optical data. Nonetheless, without particular geometrical assumptions regarding the X-ray emitting regions for each component, the measured shock parameters indicate a small volume with a high density for the decelerated shock and a large volume with a low density for the fast shock component. These density and volume ratios have also been continuously reduced. These results are in good agreement with our physical scenario of the soft X-ray production from the blast wave shock interaction with a density gradient at the boundary of the inner ring: i.e., the slow, transmitted shock into the small, dense regions of the inner ring and the fast, reflected shock off the dense CSM back into a large volume region.

The ionization timescale ($n_e t$) of the fast shock component has been relatively constant for the last ~ 6 yr (Figure 9). These $n_e t$ values are in plausible agreement with the $\sim 10 - 15$ yr old shock (the SNR age since day ~ 1200) propagating into an ambient medium of $n_e \sim$ a few 10^2 cm^{-3} (e.g., as of 2005 July, the measured $n_e t$ corresponds to $n_e \sim 500 \text{ cm}^{-3}$). Although accurate measurements of the ionization timescales of the shocked plasma are difficult with the low resolution CCD spectrum, these results are qualitatively consistent with the overall picture of the shock-ISM interaction in the SNR 1987A’s inner ring system and are also in good agreement with the results from the high resolution spectroscopy of our *Chandra*/LETG observations (Zhekov et al. 2006).

On the other hand, the increase rate of the hard band intensity ($E = 3 - 10 \text{ keV}$)

is significantly lower than that of the soft X-rays ($E = 0.5 - 2$ keV) (Table 3). This lower increase rate of the hard X-ray emission might result simply from the continuous softening of the overall X-ray spectrum. The similar morphology between the soft and the hard band images is supportive of this interpretation (Figure 3, see also Figure 4 in P05). P05, however, noticed that the hard X-ray increase rate appears to be consistent with that of radio lightcurves. A nonthermal origin for the hard X-ray emission from the synchrotron radiation in the particle acceleration sites thus cannot be ruled out (P05). On the other hand, an additional power law component is not required to adequately fit the observed X-ray spectrum. The presence of the hard power law component therefore cannot be determined with the current data because of the low photon statistics in the hard band. The true origin of the hard X-ray emission from SNR 1987A is thus currently uncertain. Although fainter than the soft band emission, the hard X-ray intensity is steadily increasing. Follow-up monitoring observations in X-rays and radio will therefore be useful to reveal the nature of the hard X-ray emission in coming years.

The authors thank P. Challis and the Supernova INTensive Study (SINS) collaboration for providing their *HST* images. We also thank K. Borkowski for providing us the updated NEI models. This work was supported in part by the Smithsonian Astrophysical Observatory under *Chandra* grant GO5-6073X.

REFERENCES

- Anders, E. & Grevesse, N. 1989, *Geochim. Cosmochim. Acta*, 53, 197
- Borkowski, K. J., Blondin, J. M., & McCray, R. 1997, *ApJ*, 477, 281
- Borkowski, K. J., Lyerly, W. J., & Reynolds, S. P. 2001, *ApJ*, 548, 820
- Bouchet, P., Dwek, E., Danziger, I. J., Arendt, R. G., De Buizer, I. J. M., Park, S., Suntzeff, N. B., Kirshner, R. P., & Challis, P. 2006, *ApJ*, in press (astro-ph/0601495)
- Burrows, C. J., Krist, J., Hester, J., Sahai, R., Trauger, J. T., Stapelfeldt, K. R., Gallagher III, J. S., Ballester, G. E., Casertano, S., Clarke, J. T., Crisp, D., Evans, R. W., Griffiths, R. E., Hoessel, J. G., Holtzman, J. A., Mould, J. R., Scowen, P. A., Watson, A. M., & Westphal, J. A. 1995, *ApJ*, 452, 680
- Burrows, D. N., Michael, E., Hwang, U., McCray, R., Chevalier, R. A., Petre, R., Garmire, G. P., Holt, S. S., & Nousek, J. A. 2000, *ApJ*, 543, L149

- Chevalier, R. A. & Dwarkadas, V. V. 1995, *ApJ*, 452, L45
- Jakobsen, P., Albrecht, R., Barbieri, C., Blades, J. C., Boksenberg, A., Crane, P., Deharveng, J. M., Disney, M. J., Kamperman, T. M., King, I. R., Macchetto, F., Mackay, C. D., Paresce, F., Weigelt, G., Baxter, D., Greenfield, P., Jedrzejewski, R., Nota, A., Sparks, W. B., Kirshner, R. P., & Panagia, N. 1991, *ApJ*, 369, L63
- Lucy, L. B. 1974, *AJ*, 79, 745
- Lundqvist, P. & Fransson, C. 1991, *ApJ*, 380, 575
- Lundqvist, P. & Fransson, C. 1996, *ApJ*, 464, 924
- Luo, D. & McCray, R. 1991, *ApJ*, 379, 659
- Luo, D., McCray, R., & Slavin, J. 1994, *ApJ*, 430, 264
- Manchester, R. N., Gaensler, B. M., Wheaton, V. C., Staveley-Mmith, L., Tzioumis, A. K., Bizunok, N. S., Kesteven, M. J., & Reynolds, J. E. 2002, *PASA*, 19, 207
- Michael, E., McCray, R., Pun, C. S. J., Garnavich, P., Challis, P., Kirshner, R. P., Raymond, J., Borkowski, K., Chevalier, R., Filippenko, A. V., Fransson, C., Lundqvist, P., Panagia, N., Phillips, M. M., Sonneborn, G., Suntzeff, N. B., Wang, L., & Wheeler, J. C. 2000, *ApJ*, 542, L53
- Michael, E., Zhekov, S. A., McCray, R., Hwang, U., Burrows, D. N., Park, S., Garmire, G. P., Holt, S. S., & Hasinger, G., 2002, *ApJ*, 574, 166
- Mori, K., Tsunemi, H., Miyata, E., Baluta, C. J., Burrows, D. N., Garmire, G. P., & Chartas, G. 2001, in “New Century of X-Ray Astronomy”, *ASP Conf. Ser.*, eds. H. Inoue and H. Kunieda (San Francisco: ASP), 251, 576
- Park, S., Burrows, D. N., Garmire, G. P., Nousek, J. A., McCray, R., Michael, E., & Zhekov, S. A. 2002, *ApJ*, 567, 314
- Park, S., Zhekov, S. A., Burrows, D. N., Garmire, G. P., & McCray, R. 2004, *ApJ*, 610, 275
- Park, S., Zhekov, S. A., Burrows, D. N., Garmire, G. P. & McCray, R. 2005a, *AdSpR*, 35, 991
- Park, S., Zhekov, S. A., Burrows, D. N., & McCray, R. 2005b, *ApJ*, 634, L73 (P05)
- Richardson, W. H. 1972, *J. Opt. Soc. Am.*, 62, 55

- Russell, S. C. & Dopita, M. A. 1992, *ApJ*, 384, 508
- Smith, R. K., Brickhouse, N. S., Liedahl, D. A., & Raymond, J. C. 2001, *ApJ*, 556, L91
- Sugerman, B. E. K., Lawrence, S. S., Crofts, A. P. S., Bouchet, P., & Heathcote, S. R. 2002, *ApJ*, 572, 209
- Townsley, L. K., Broos, P. S., Garmire, G. P., & Nousek, J. A. 2000, *ApJ*, 534, L139
- Townsley, L. K., Broos, P. S., Chartas, G., Moskalenko, E., Nousek, J. A., & Pavlov, G. G. 2002a, *Nucl. Instrum. Methods Phys. Res. A*, 486, 716
- Townsley, L. K., Broos, P. S., Nousek, J. A., & Garmire, G. P. 2002b, *Nucl. Instrum. Methods Phys. Res. A*, 486, 751
- Tsunemi, H., Mori, K., Miyata, E., Baluta, C., Burrows, D. N., Garmire, G. P., & Chartas, G. 2001, *ApJ*, 554, 496
- Zhekov, S. A., McCray, R., Borkowski, K. J., Burrows, D. N., & Park, S. 2005, *ApJ*, 628, L127
- Zhekov, S. A., McCray, R., Borkowski, K. J., Burrows, D. N., & Park, S. 2006, *ApJ*, in press (astro-ph/0603305)

Table 1. Chandra Observations of SNR 1987A.

Observation ID	Date (Age ^a)	Instrument	Exposure (ks)	Counts
124+1387 ^b	1999-10-6 (4609)	ACIS-S + HETG	116.1	690 ^c
122	2000-1-17 (4711)	ACIS-S3	8.6	607
1967	2000-12-07 (5038)	ACIS-S3	98.8	9030
1044	2001-4-25 (5176)	ACIS-S3	17.8	1800
2831	2001-12-12 (5407)	ACIS-S3	49.4	6226
2832	2002-5-15 (5561)	ACIS-S3	44.3	6427
3829	2002-12-31 (5791)	ACIS-S3	49.0	9277
3830	2003-7-8 (5980)	ACIS-S3	45.3	9668
4614	2004-1-2 (6157)	ACIS-S3	46.5	11856
4615	2004-7-22 (6359)	ACIS-S3 (1/2 subarray)	48.8	17979
4640+4641+5362 +5363+6099 ^b	2004-8-26~9-5 (~6400)	ACIS-S + LETG	289.0	16557 ^c
5579+6178 ^b	2005-1-12 (6533)	ACIS-S3 (1/8 subarray)	48.3	24939
5580+6345 ^b	2005-7-14 (6716)	ACIS-S3 (1/8 subarray)	44.1	27048

^aDay since SN.

^bThese observations were splitted by multiple sequences which were combined for the analysis.

^cPhoton statistics are from the zeroth-order data.

Table 2. Best-fit Parameters from the Two-Shock Model Fit of SNR 1987A^a

Age ^b (Days)	$kT(\text{soft})^c$ (keV)	$kT(\text{hard})^c$ (keV)	$n_e t(\text{hard})^c$ ($10^{11} \text{ cm}^{-3} \text{ s}$)	$EM(\text{soft})^c$ (10^{57} cm^{-3})	$EM(\text{hard})^c$ (10^{57} cm^{-3})	χ^2/ν
4711 ^d	$0.222^{+0.032}_{-0.029}$	$3.38^{+2.82}_{-1.20}$	2.68 (fixed)	$24.00^{+6.00}_{-6.30}$	$4.44^{+0.87}_{-0.66}$	19.0/21
5038	$0.228^{+0.011}_{-0.006}$	$3.16^{+0.49}_{-0.33}$	$1.85^{+0.54}_{-0.39}$	$39.60^{+3.00}_{-5.40}$	$5.37^{+0.45}_{-0.39}$	96.0/98
5176 ^d	$0.235^{+0.017}_{-0.015}$	$3.57^{+1.33}_{-0.96}$	2.00 (fixed)	$47.09^{+7.20}_{-6.00}$	$5.73^{+0.72}_{-0.54}$	22.8/41
5407	$0.238^{+0.056}_{-0.008}$	$2.98^{+0.74}_{-0.46}$	$2.01^{+1.05}_{-0.57}$	$58.49^{+4.80}_{-26.40}$	$7.59^{+0.99}_{-0.87}$	78.4/76
5561	$0.251^{+0.049}_{-0.009}$	$3.18^{+0.63}_{-0.62}$	$2.02^{+1.09}_{-0.56}$	$64.49^{+7.80}_{-26.70}$	$8.55^{+1.17}_{-0.78}$	62.8/78
5791	$0.269^{+0.045}_{-0.029}$	$3.14^{+0.68}_{-0.34}$	$1.81^{+0.61}_{-0.47}$	$77.09^{+26.10}_{-24.00}$	$10.59^{+0.99}_{-1.14}$	92.8/100
5980	$0.272^{+0.078}_{-0.017}$	$2.73^{+0.38}_{-0.28}$	$3.39^{+2.07}_{-1.12}$	$89.69^{+21.30}_{-39.00}$	$13.74^{+1.47}_{-1.44}$	122.2/101
6157	$0.263^{+0.021}_{-0.009}$	$2.75^{+0.33}_{-0.22}$	$3.11^{+1.30}_{-0.84}$	$121.18^{+15.00}_{-23.40}$	$16.74^{+1.50}_{-1.44}$	132.4/109
6359	$0.284^{+0.044}_{-0.010}$	$2.25^{+0.20}_{-0.19}$	$2.69^{+0.92}_{-0.60}$	$160.48^{+25.20}_{-26.10}$	$23.31^{+1.65}_{-1.83}$	167.7/123
6533	$0.303^{+0.065}_{-0.025}$	$2.25^{+0.19}_{-0.20}$	$2.09^{+0.65}_{-0.39}$	$202.47^{+58.49}_{-67.49}$	$27.51^{+2.28}_{-1.68}$	109.0/133
6716	$0.309^{+0.051}_{-0.025}$	$2.30^{+0.20}_{-0.17}$	$2.61^{+0.77}_{-0.55}$	$255.87^{+63.59}_{-68.39}$	$30.96^{+2.64}_{-2.16}$	151.9/135

^a N_H is fixed at $2.35 \times 10^{21} \text{ cm}^{-2}$.

^bDays since the SN.

^c 2σ uncertainties.

^dThe errors are estimated with $n_e t$ parameters fixed at the best-fit values.

Table 3. X-Ray Luminosity of SNR 1987A^a

Age ^b (Days)	L_X (0.5–2.0 keV) (10^{35} ergs s ⁻¹)	L_X (3–10 keV) (10^{35} ergs s ⁻¹)	L_X (0.5–10 keV) (10^{35} ergs s ⁻¹)
4711	1.13	0.26	1.54
5038	1.76	0.28	2.22
5176	2.02	0.37	2.59
5407	2.62	0.37	3.24
5561	3.05	0.45	3.79
5791	4.14	0.55	5.05
5980	4.69	0.59	5.71
6157	5.58	0.73	6.82
6359	8.14	0.76	9.54
6533	11.97	0.85	13.58
6716	14.19	0.99	16.06

^aAfter corrected for $N_H = 2.35 \times 10^{21}$ cm⁻².

^bDays since the SN.

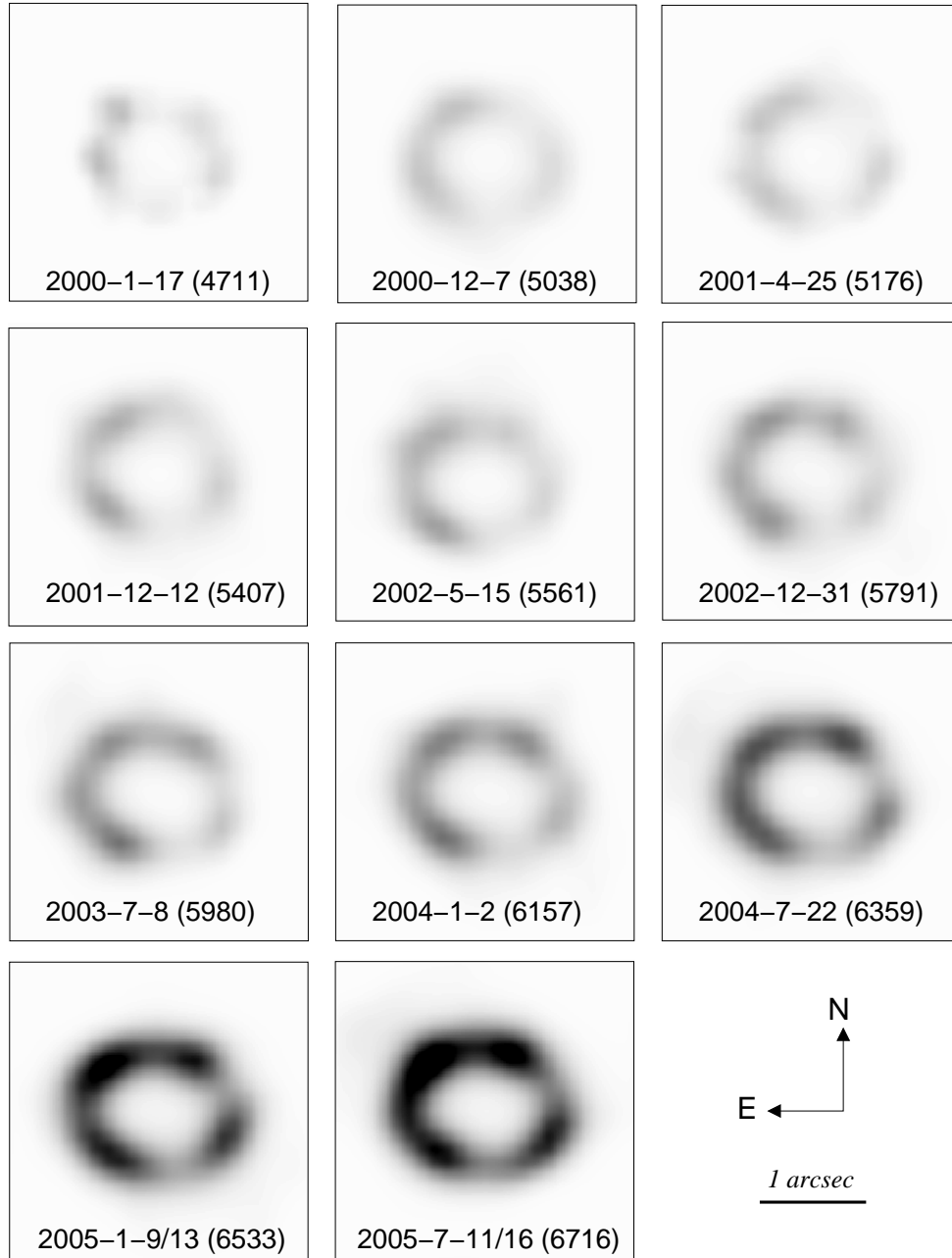


Fig. 1.— The 0.3–8.0 keV broadband images of SNR 1987A. Each image is exposure-corrected and the darker gray-scales correspond to higher intensities. The image deconvolution has been applied and then the images have been smoothed by convolving with a Gaussian ($\sim 0''.1$ FWHM). In each panel, the observation date and the age (day since the SN, in the parentheses) of the SNR are presented.

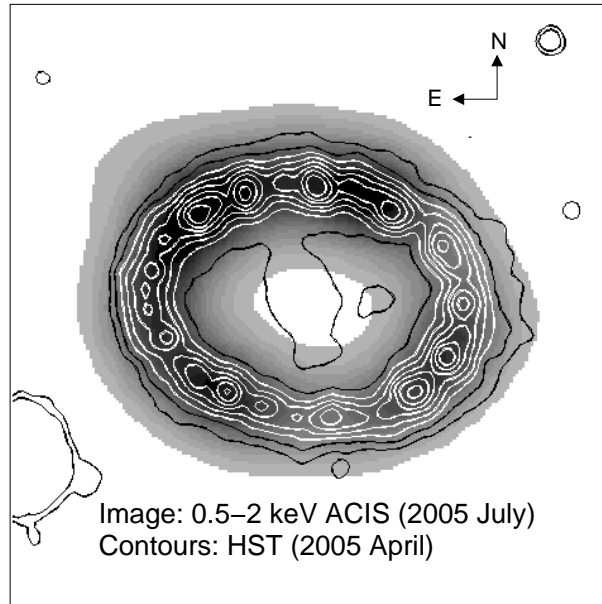


Fig. 2.— The soft X-ray (0.5–2 keV) image from the latest ACIS observations (taken in 2005 July) overlaid with the optical image contours (taken in 2005 April) from *the Hubble Space Telescope (HST)*. The unpublished *HST* data have been provided by Peter Challis.

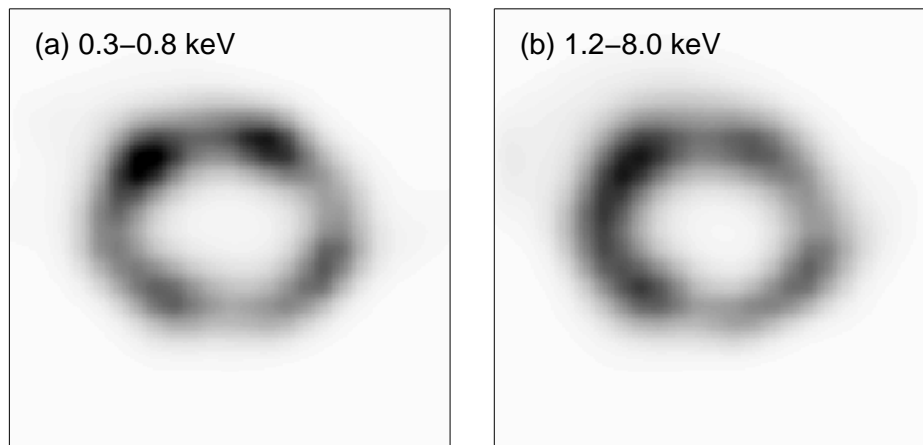


Fig. 3.— (a) The 0.3 – 0.8 keV and (b) 1.2 – 8 keV subband images of SNR 1987A as of 2005 July. Each image has been processed in the same way as those in Figure 1. The image orientation is also the same as Figure 1.

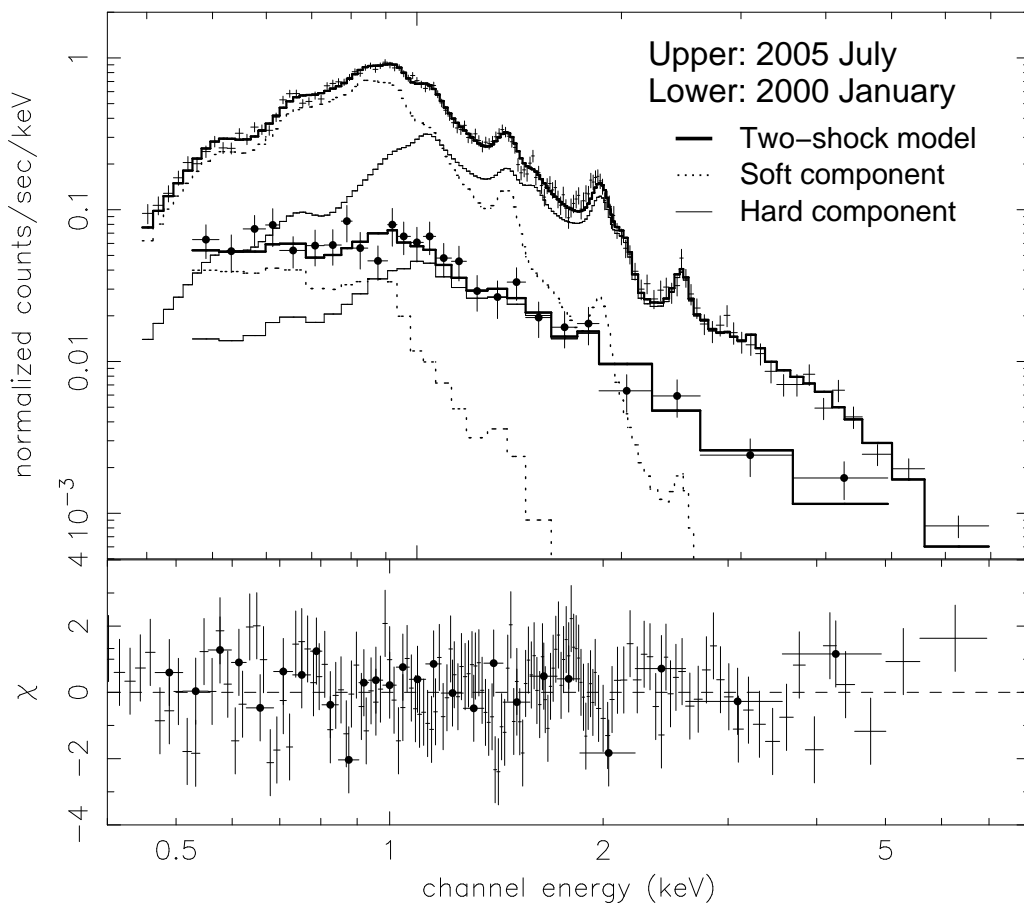


Fig. 4.— X-ray spectrum of SNR 1987A as obtained with the ACIS-S3. The spectrum in two epochs are representatively displayed. The upper plot is the 2005-July spectrum (no markers) and the lower plot (filled circles) is 2000-January spectrum. The overlaid thick-solid lines are the best-fit two-shock model for each spectrum. For each spectrum, the soft and the hard sub-components of the best-fit two-shock model are also overlaid. The upper dotted line is the soft component for the 2005-July spectrum, and the lower dotted line is the soft component for 2000-January spectrum. The upper and lower thin-solid lines are the hard component for the 2005-July and the 2000-January spectrum, respectively.

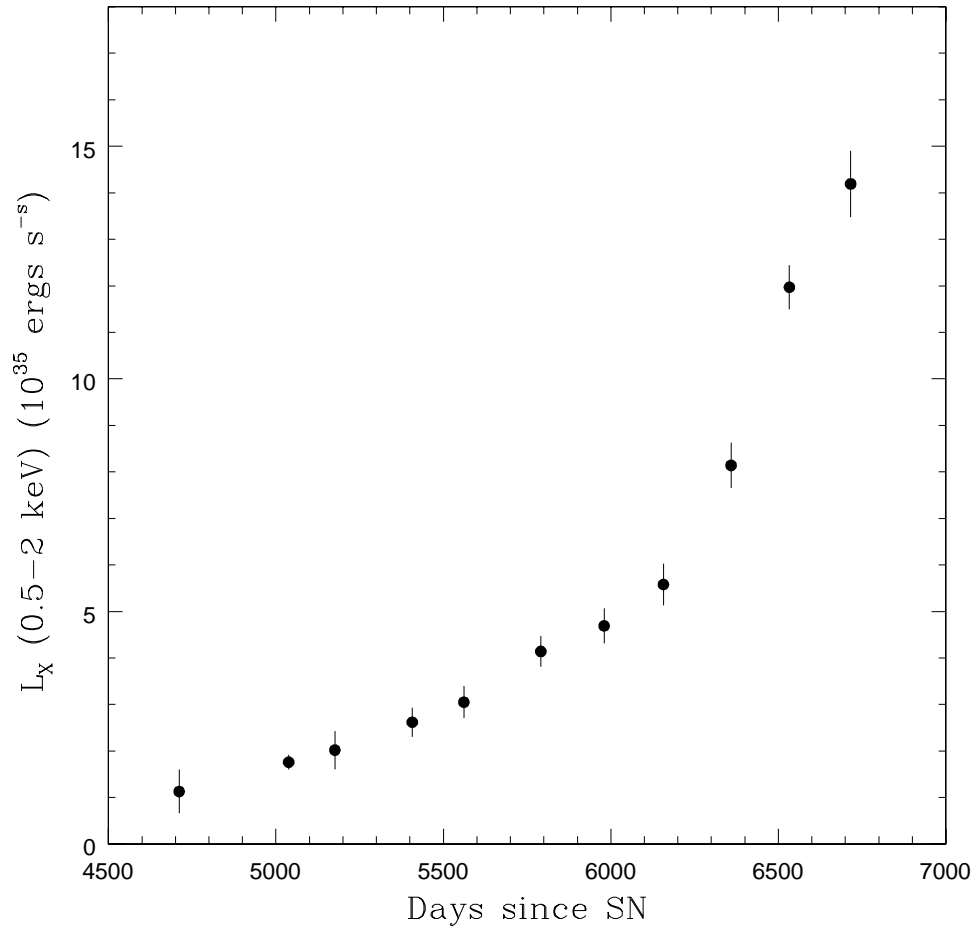


Fig. 5.— The 0.5 – 2 keV band soft X-ray lightcurve of SNR 1987A as presented in Table 3.

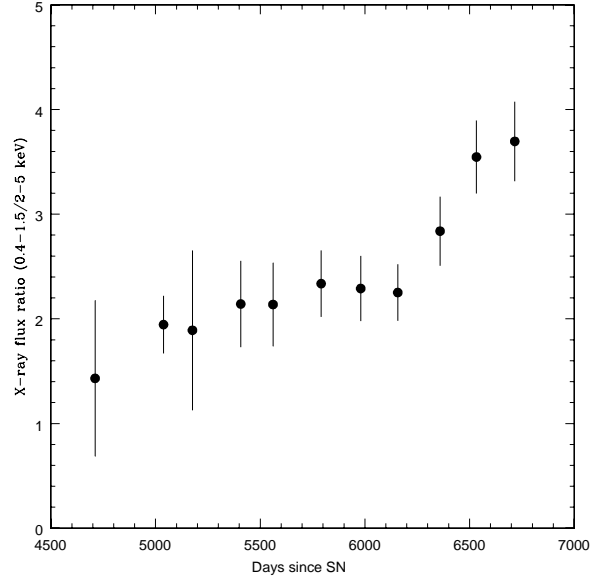


Fig. 6.— The observed 0.4–1.5 to 2–5 keV band X-ray flux ratio of SNR 1987A.

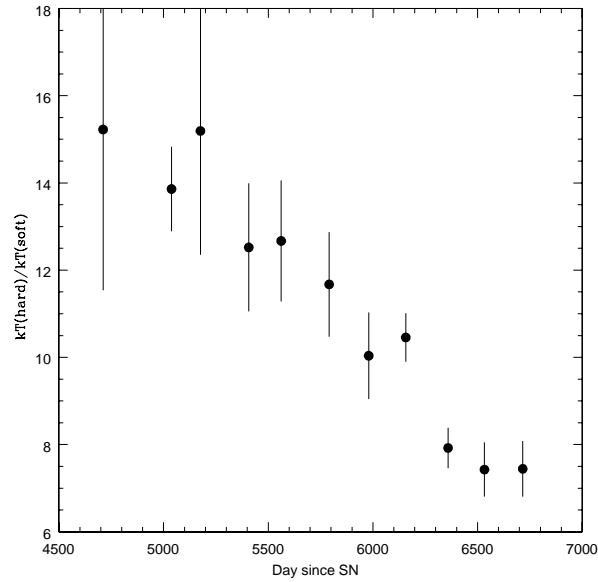


Fig. 7.— The electron temperature ratios between the hard and the soft component shocks from SNR 1987A.

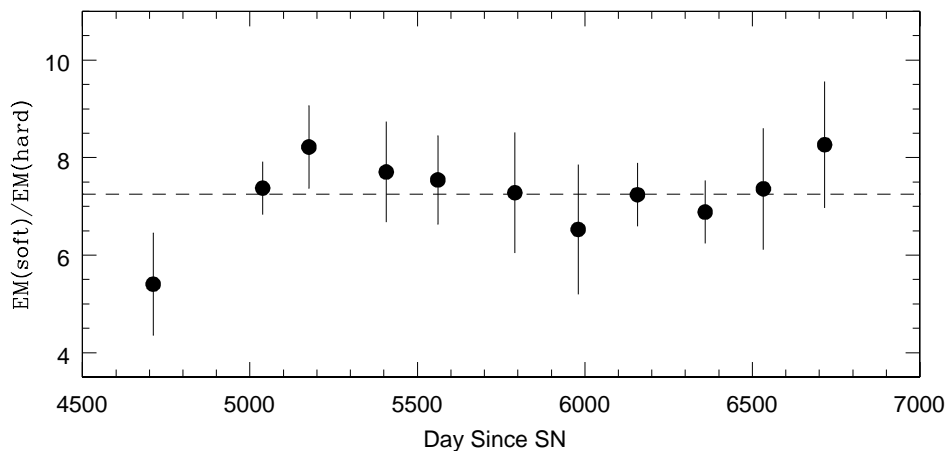


Fig. 8.— The emission measure ratios between the soft and the hard component shocks from SNR 1987A. The horizontal dashed line represents the average ratio.

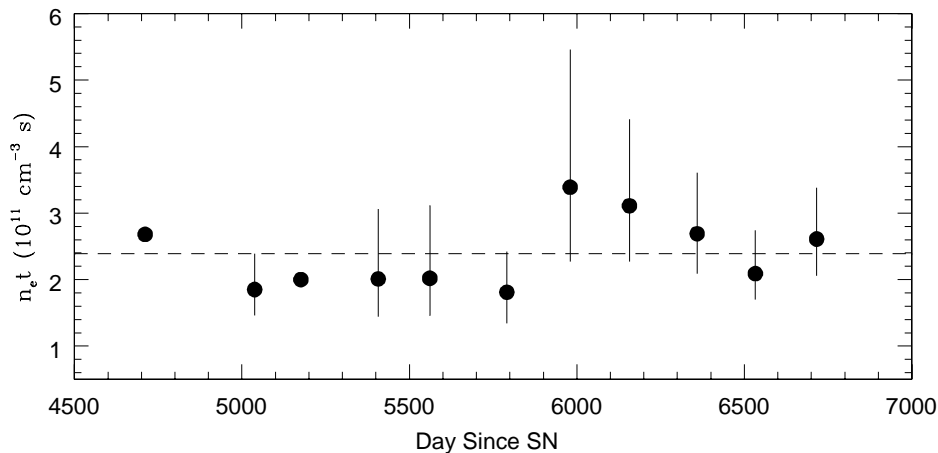


Fig. 9.— The ionization timescale ($n_e t$) of the hard component of SNR 1987A spectrum. The horizontal dashed line represents the average $n_e t$ value. Note that $n_e t$ for two epochs (day 4711 and 5176) is unconstrained because of the poor photon statistics. Only the “best-fit” values are presented for them without error bars.